

Ultracold collisions in magnetic fields: reducing inelastic cross sections near Feshbach resonances

R. Adam Rowlands and Jeremy M. Hutson

Department of Chemistry, University of Durham, South Road, Durham, DH1 3LE, England

Maykel Leonardo González-Martínez

Departamento de Física General, InSTEC, Habana 6163, Cuba

(Dated: November 23, 2018)

We have carried out bound-state and low-energy quantum scattering calculations on $\text{He} + \text{NH}$ ($^3\Sigma^-$) in magnetic fields, with the NH molecule in its $n = 1$ rotationally excited states. We have explored the pattern of levels as a function of magnetic field and identified the nearly good quantum numbers in different regimes. We have used the bound-state calculations to locate low-energy Feshbach resonances. When the magnetic field is used to tune across such a resonance, the real and imaginary part of the scattering length show asymmetric oscillations and peaks with amplitude between 1 and 3 Å. The scattering length does *not* pass through a pole at resonance. The resonant behavior is characterized by a complex resonant scattering length a_{res} . The corresponding inelastic cross sections show troughs as well as peaks near resonance. This may be important for efforts to achieve evaporative and sympathetic cooling for molecules, because it offers the hope that inelastic trap losses can be reduced by tuning close to a Feshbach resonance.

PACS numbers: 34.50.-s, 34.10.+x, 03.65.Nk, 82.20.Xr, 34.30.+h

I. INTRODUCTION

Collisions between ultracold atoms can be controlled by tuning the atomic interactions using applied magnetic fields [1, 2]. Such techniques have been used to cause controlled implosion of Bose-Einstein condensates [3] and to produce dimers of both bosonic [4, 5, 6, 7] and fermionic [8, 9, 10, 11] alkali metal atoms. Long-lived molecular Bose-Einstein condensates of fermion dimers have been produced [12, 13, 14], and the first signatures of ultracold triatomic [15] and tetraatomic [16] molecules have been observed. It is proving possible to move molecules selectively between quantum states by either fast or slow sweeps of magnetic fields across avoided crossings between bound states [17, 18].

The overall strength of the interaction between a pair of atoms is characterized by the scattering length a [19]. An important feature of elastic scattering in ultracold atomic gases is that a passes through a pole as the magnetic field B is swept across a Feshbach resonance at constant kinetic energy [20],

$$a(B) = a_{\text{bg}} \left[1 - \frac{\Delta_B}{B - B_{\text{res}}} \right], \quad (1)$$

where a_{bg} is a near-constant background scattering length and B_{res} and Δ_B are the position and width of the resonance. The scattering length can thus be tuned to any desired value, positive or negative. Positive values correspond to interactions that are overall repulsive and negative values to interactions that are overall attractive. The elastic cross section is given by

$$\sigma_{\text{el}} = \frac{4\pi a^2}{1 + k^2 a^2}, \quad (2)$$

where the kinetic energy is $E_{\text{kin}} = \hbar^2 k^2 / (2\mu)$ and μ is the reduced mass for the collision. The elastic cross section thus passes through a peak of height $4\pi/k^2$ at resonance.

It has recently become possible to cool molecules directly from high temperature to the millikelvin regime, using methods such as buffer-gas cooling [21, 22, 23] and Stark deceleration [24, 25]. Polar molecules such as ND_3 and OH have been successfully trapped at temperatures around 10 mK, and there are a variety of proposals for ways to cool them further, including evaporative cooling, sympathetic cooling and cavity-assisted cooling [26, 27, 28]. Very recently, NH has been trapped at temperatures around 0.7 K by buffer-gas cooling in cryogenic helium.

In previous work [29], we have explored the possibility of controlling *molecular* interactions in the same way as atomic interactions. We have generalised the BOUND [30] and MOLSCAT [31] packages to carry out bound-state calculations and quantum scattering calculations in applied magnetic fields for systems made up of a $^{2S+1}\Sigma$ molecule and a structureless atom.

In our initial calculations on $\text{He} + \text{NH}$ ($^3\Sigma$) [29], we used BOUND to locate magnetic fields at which bound states cross open-channel thresholds. We then used MOLSCAT to characterize the resulting low-energy Feshbach resonances as a function of magnetic field. For a resonance at which a bound state crossed the *lowest* open-channel threshold, we observed a pole in the scattering length that followed Eq. 1. However, for a resonance in which a state crossed a *higher* threshold, we observed quite different behavior. The scattering length showed only a weak oscillation instead of a pole. The suppression of the pole was attributed to inelastic effects. The calculations were for NH in its lowest rotational state ($n = 0$), for which inelastic coupling is very weak, and

the resonances were very narrow, but even so the amplitude of the oscillation in $a(B)$ was only about 9 Å.

A full derivation of the resonant behavior of the scattering length in the presence of inelastic effects has been given previously [32], so only a brief version will be given here to explain the basic physics and define notation. In the presence of inelastic collisions, the scattering matrix S that describes the collision in quantum-mechanical terms has elements $S_{ii'}$. The diagonal S-matrix element in the incoming channel 0 has magnitude $|S_{00}| \leq 1$ and may be written in terms of a complex phase shift δ_0 with a positive imaginary part [33],

$$S_{00}(k_0) = e^{2i\delta_0(k_0)}, \quad (3)$$

where k_0 is the wave vector in the incoming channel. This can be expressed in terms of a complex energy-dependent scattering length, $a(k_0) = \alpha(k_0) - i\beta(k_0)$ [34, 35], defined as

$$a(k_0) = \frac{-\tan \delta_0(k_0)}{k_0} = \frac{1}{ik_0} \left(\frac{1 - S_{00}(k_0)}{1 + S_{00}(k_0)} \right). \quad (4)$$

$a(k_0)$ becomes constant at limitingly low kinetic energy. The elastic and total inelastic cross sections are exactly [36]

$$\sigma_{\text{el}}(k_0) = \frac{4\pi|a|^2}{1 + k_0^2|a|^2 + 2k_0\beta} \quad (5)$$

and

$$\sigma_{\text{inel}}^{\text{tot}}(k_0) = \frac{4\pi\beta}{k_0(1 + k_0^2|a|^2 + 2k_0\beta)}. \quad (6)$$

A scattering resonance is most simply characterized in terms of the S-matrix eigenphase sum Σ , which is the sum of phase shifts obtained from the eigenvalues of the S matrix [37, 38]. The eigenphase sum is a real quantity, and across a resonance follows the Breit-Wigner form,

$$\Sigma(B) = \Sigma_{\text{bg}} + \tan^{-1} \left[\frac{\Gamma_B}{2(B_{\text{res}} - B)} \right], \quad (7)$$

where Σ_{bg} is a slowly varying background term, B_{res} is the resonance position and Γ_B is a resonance width (not the same as Δ_B in Eq. 1). The B subscripts indicate that we are considering the resonance as a function of magnetic field rather than energy. The individual S-matrix elements describe circles in the complex plane [32, 39, 40, 41],

$$S_{ii'}(B) = S_{\text{bg},ii'} - \frac{ig_{Bi}g_{Bi'}}{B - B_{\text{res}} + i\Gamma_B/2}, \quad (8)$$

where g_{Bi} is complex. The radius of the circle in S_{ii} is $|g_{Bi}^2/\Gamma_B|$. The *partial width* Γ_{Bi} for channel i is usually defined as a real quantity, but here we also need a corresponding phase ϕ_i to describe the *orientation* of the circle in the complex plane, $g_{Bi}^2 = \Gamma_{Bi}e^{2i\phi_i}$. The width Γ_B and partial widths Γ_{Bi} are signed quantities, positive if the

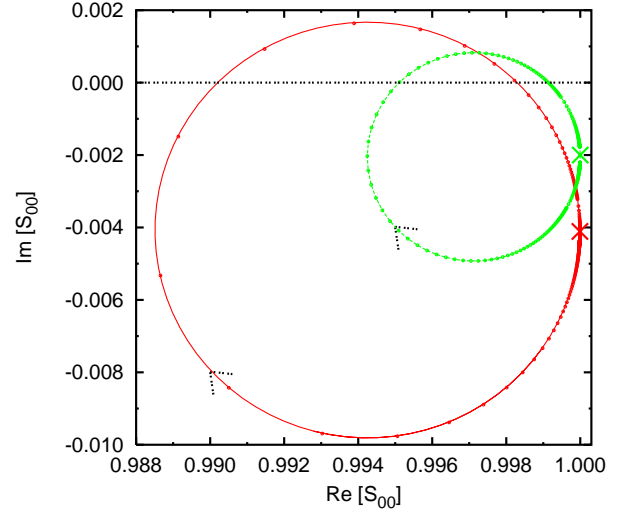


FIG. 1: (Color online). The small circles in the elastic S-matrix elements in the presence of inelastic scattering for He + NH ($n = 0$) scattering at $E_{\text{kin}} = 10^{-6}$ K (green, smaller circle) and 4×10^{-6} K (red, larger circle). Reproduced with permission from ref. 29.

resonant state tunes downwards across the threshold as a function of B and negative if it tunes upwards. For a narrow resonance, the total width is just the sum of the partial widths,

$$\Gamma_B = \sum_i \Gamma_{Bi}. \quad (9)$$

The partial widths for *elastic* channels (degenerate with the incoming channel) are proportional to k_0 at low energy. We may define a reduced partial width γ_{B0} for the incoming channel by

$$\Gamma_{B0}(k_0) = 2k_0\gamma_{B0}, \quad (10)$$

and the reduced width is independent of k_0 at low energy (typically below $E_{\text{kin}} = 1$ mK). By contrast, the partial widths for *inelastic* channels depend on open-channel wavefunctions with large wave vectors k_i and are effectively independent of k_0 in the ultracold regime. If the inelastic partial widths Γ_{Bi} are non-zero, they eventually dominate Γ_{B0} as k_0 decreases. The radius of the circle (8) described by S_{00} thus drops linearly to zero as k_0 decreases, as shown in Figure 1. This is *qualitatively different* from the behavior in the absence of inelastic channels, where the circle has radius 1 even at limitingly low energy.

The radius of the circle in S_{00} is Γ_{B0}/Γ_B . For small k_0 , where Eq. 10 applies, this is approximately $2k_0\gamma_{B0}/\Gamma_B^{\text{inel}}$. The formula followed by the complex scattering length is

$$a(B) = a_{\text{bg}} + \frac{a_{\text{res}}}{2(B - B_{\text{res}})/\Gamma_B^{\text{inel}} + i}, \quad (11)$$

where Γ_B^{inel} is the energy-independent part of Γ_B (omitting Γ_{B0}) and a_{res} is a *resonant scattering length* that

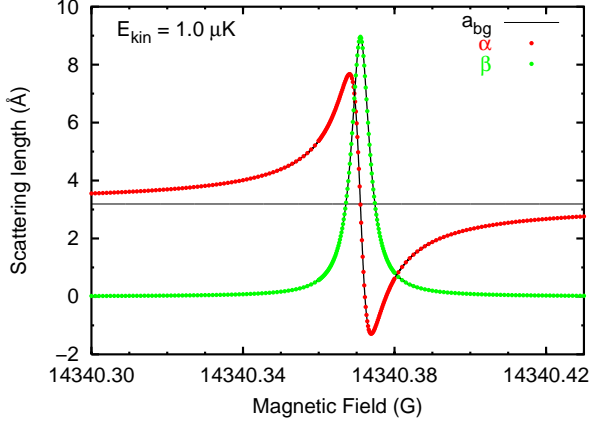


FIG. 2: (Color online). Real and imaginary parts of the scattering length across a Feshbach resonance in He + NH ($n = 0$), showing a small symmetrical oscillation in the real part (red) and a peak in the imaginary part (green). Reproduced with permission from ref. 32.

characterizes the strength of the resonance,

$$a_{\text{res}} = \frac{2\gamma B_0}{\Gamma_B^{\text{inel}}} e^{2i(\phi_0 + k_0 \alpha_{\text{bg}})}. \quad (12)$$

Both a_{res} and the background term a_{bg} can in general be complex and are independent of k_0 at low energy. However, in the special case where the background scattering is purely elastic (a_{bg} is real), unitarity requires that the circle in S_{00} must loop towards the origin as shown in the upper panel of Fig. 3. This requires that a_{res} is also real. Across the width of the resonance, the real part $\alpha(B)$ of the scattering length $a(B)$ then oscillates about a_{bg} by $\pm a_{\text{res}}/2$ and the imaginary part peaks at $\beta(B) = a_{\text{res}}$. This was the behavior seen for $a(B)$ in ref. 29 for He + NH($^3\Sigma$) collisions with NH in $n = 0$ states, shown in Fig. 2.

The purpose of the present work is to explore a rather more complicated case, with significant background inelastic scattering. Eq. 11 still holds, but a_{res} can be complex and the circle in S_{00} then does not point directly towards the origin. This behavior is shown in the lower panel of Fig. 3. The elastic cross section is given by

$$\sigma_{\text{el}}(B) = \frac{\pi}{k_0^2} |1 - S_{00}(k_0)|^2, \quad (13)$$

so at any value of B it depends on the distance between S_{00} and the point X at $S_{00} = +1$. However, the total inelastic cross section is given by

$$\sigma_{\text{inel}}^{\text{tot}}(B) = \frac{\pi}{k_0^2} (1 - |S_{00}(k_0)|^2), \quad (14)$$

and thus depends on the distance of S_{00} from the unit circle. If the circle in S_{00} does not point directly towards the origin, it is clear from Fig. 3 that the total inelastic cross section can show a trough as well as a peak near

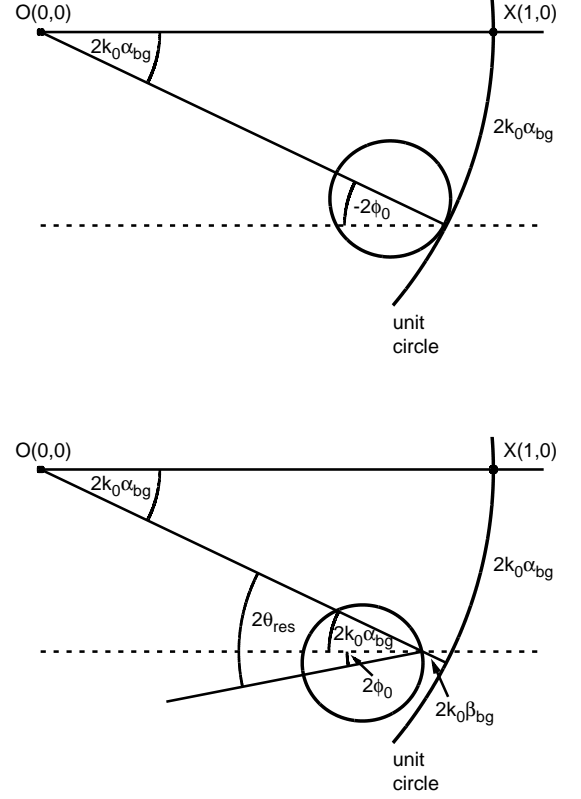


FIG. 3: The distinction between an S-matrix circle in the complex plane that points directly towards the origin O (top) and one that does not (bottom), showing the relationship between θ_{res} and ϕ_0 .

resonance. This offers the hope that resonances can be used to *reduce* inelastic rates as well as increase them.

In the general case, the explicit expressions for the real and imaginary parts of $a(B)$ are [32]

$$\begin{aligned} \alpha(B) &= \alpha_{\text{bg}} + \frac{\alpha_{\text{res}} [2(B - B_{\text{res}})/\Gamma_B^{\text{inel}}] - \beta_{\text{res}}}{[2(B - B_{\text{res}})/\Gamma_B^{\text{inel}}]^2 + 1}, \\ \beta(B) &= \beta_{\text{bg}} + \frac{\alpha_{\text{res}} + \beta_{\text{res}} [2(B - B_{\text{res}})/\Gamma_B^{\text{inel}}]}{[2(B - B_{\text{res}})/\Gamma_B^{\text{inel}}]^2 + 1}, \end{aligned} \quad (15)$$

where $a(B) = \alpha(B) - i\beta(B)$ and similarly for a_{res} and a_{bg} . The peak profiles for the elastic and total inelastic cross sections are given by combining these with Eqs. 5 and 6.

Some useful properties of the scattering length and cross sections follow from simple geometrical considerations. The complex scattering length $a(B)$ has a value a_{bg} far from resonance and describes a circle of radius $|a_{\text{res}}|/2$ in the complex plane as B is tuned across the resonance. If we write the resonant scattering length as

$$a_{\text{res}} = |a_{\text{res}}| \exp(2i\theta_{\text{res}}), \quad (16)$$

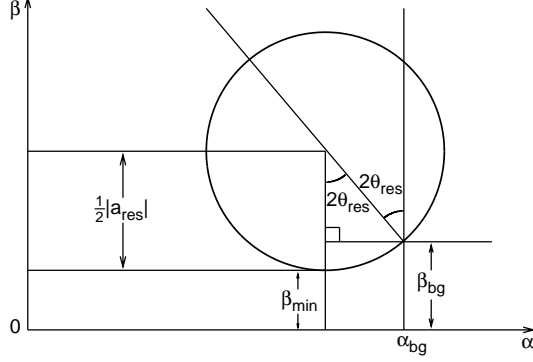


FIG. 4: The resonant circle in the complex scattering length, showing the extent to which the imaginary part of a_{res} can reduce inelastic scattering.

where $\theta_{\text{res}} = \phi_0 + k_0 \alpha_{\text{bg}}$, then the circle is as shown in Fig. 4. The smallest value achieved by $\beta(B)$ is

$$\beta_{\text{min}} = \beta_{\text{bg}} - \frac{1}{2}|a_{\text{res}}|(1 - \cos 2\theta_{\text{res}}), \quad (17)$$

which occurs at $B_{\text{min}} = B_{\text{res}} + x_{\text{min}} \Gamma_B^{\text{inel}}/2$ with

$$x_{\text{min}} = -(\alpha_{\text{res}}/\beta_{\text{res}}) - [(\alpha_{\text{res}}/\beta_{\text{res}})^2 + 1]^{1/2}. \quad (18)$$

This defines the smallest value of the total inelastic cross section through Eq. 5. Unitarity requires that $|S_{00}| \leq 1$ and $\beta(B) \geq 0$, so the limits on the possible values of θ_{res} are

$$\cos 2\theta_{\text{res}} \geq \cos 2\theta_{\text{res}}^{\text{max}} = 1 - \frac{2\beta_{\text{bg}}}{|a_{\text{res}}|}. \quad (19)$$

An obvious special case of this is that, if a_{bg} is real, $\theta_{\text{res}} = 0$ so that a_{res} is also real.

Some examples of the possible behavior are illustrated in Fig. 5 for a case with moderately strong background inelasticity, $\beta_{\text{bg}} = |a_{\text{res}}|/2$ and $|\alpha_{\text{bg}}| = 2|a_{\text{res}}|$. For these parameters, $\cos \theta_{\text{res}}^{\text{max}} = 0$. When θ_{res} is close to its maximum value, $\beta(B)$ dips close to zero and the total inelastic cross section shows a trough that can reduce inelastic collision rates by more than a factor of 10. The elastic cross section also oscillates, but if $|a_{\text{res}}| \ll |\alpha_{\text{bg}}|$ the oscillation is relatively weak and if α_{bg} and β_{res} have opposite signs it is peak-like rather than trough-like.

II. RESONANCES IN HE + NH ($n = 1$)

We have carried out bound-state and scattering calculations on He + NH ($n = 1$) in a magnetic field using methods almost identical to those used previously for $n = 0$ [29]. The bound-state Schrödinger equation was solved using the BOUND package [30], as modified to handle magnetic fields [29]. In the presence of a

magnetic field, the total angular momentum is no longer a good quantum number. The calculations are therefore carried out in a completely decoupled basis set, $|nm_n\rangle|sm_s\rangle|Lm_L\rangle$, where $s = 1$ is the electron spin of NH and L is the end-over-end rotational angular momentum of He about NH. All the m quantum numbers represent space-fixed projections on the axis defined by the magnetic field. The only good quantum numbers are the parity $(-1)^{n+L+1}$ and the total projection quantum number $M_{\text{tot}} = m_n + m_s + m_L$.

BOUND propagates a set of coupled differential equations outwards from a point R_{min} , deep inside the inner classically forbidden region, and inwards from a boundary point R_{max} at long range. The two solutions meet at a matching point R_{mid} , and bound-state eigenvalues are found by locating values of the energy for which the inward and outward solutions can be matched. The procedure used by BOUND is to seek energies at which one of the eigenvalues of the log-derivative matching matrix is zero [42].

For true bound states, R_{max} can be placed in the outer classically forbidden region. However, in the present work we are dealing with states of He-NH that lie close to the $n = 1$ threshold and are thus more than 30 cm^{-1} above the $n = 0$ thresholds. Since there are open channels, these are actually quasibound states and can predissociate to form He + NH ($n = 0$). Nevertheless, they can still be located by artificially applying a *bound state* boundary condition at R_{max} , and this is how BOUND is used in the present work.

Applying a bound-state boundary condition has the side-effect of box-quantizing the continuum states above both the $n = 0$ and $n = 1$ thresholds. The resulting *artificial* bound states are easily identified because their energies depend on R_{max} . Difficulties arise only if an artificial bound state lies accidentally close to the level of interest, in which case the two states can perturb one another. Fig. 6 shows an example of artificial levels crossing the real levels as a function of R_{max} . For the case of He-NH it was usually possible to estimate the positions of the physical bound levels to within 0.01 cm^{-1} . The perturbations are a measure of the genuine couplings to the continuum and are comparable to the width of the quasibound state, so this accuracy is sufficient for use in locating resonance positions.

Fig. 7 shows the quasibound states of He-NH near the $n = 1$ threshold with artificial levels removed. Crossings between quasibound states and thresholds will produce zero-energy Feshbach resonances in s-wave scattering if an $L = 0$ scattering channel is permitted by the constraints on parity and M_{tot} . For $M_{\text{tot}} = 0$ this occurs only for thresholds corresponding to $m_j = 0$, as shown by the circles in Fig. 7.

Each NH monomer level with $n = 1$ is split into 3 components with $j = 0, 1$ and 2 by coupling to the spin $s = 1$. The He-NH levels closest to the $n = 1$ thresholds have predominantly $L = 2$ character. At zero field the total angular momentum J is a good quantum number, so

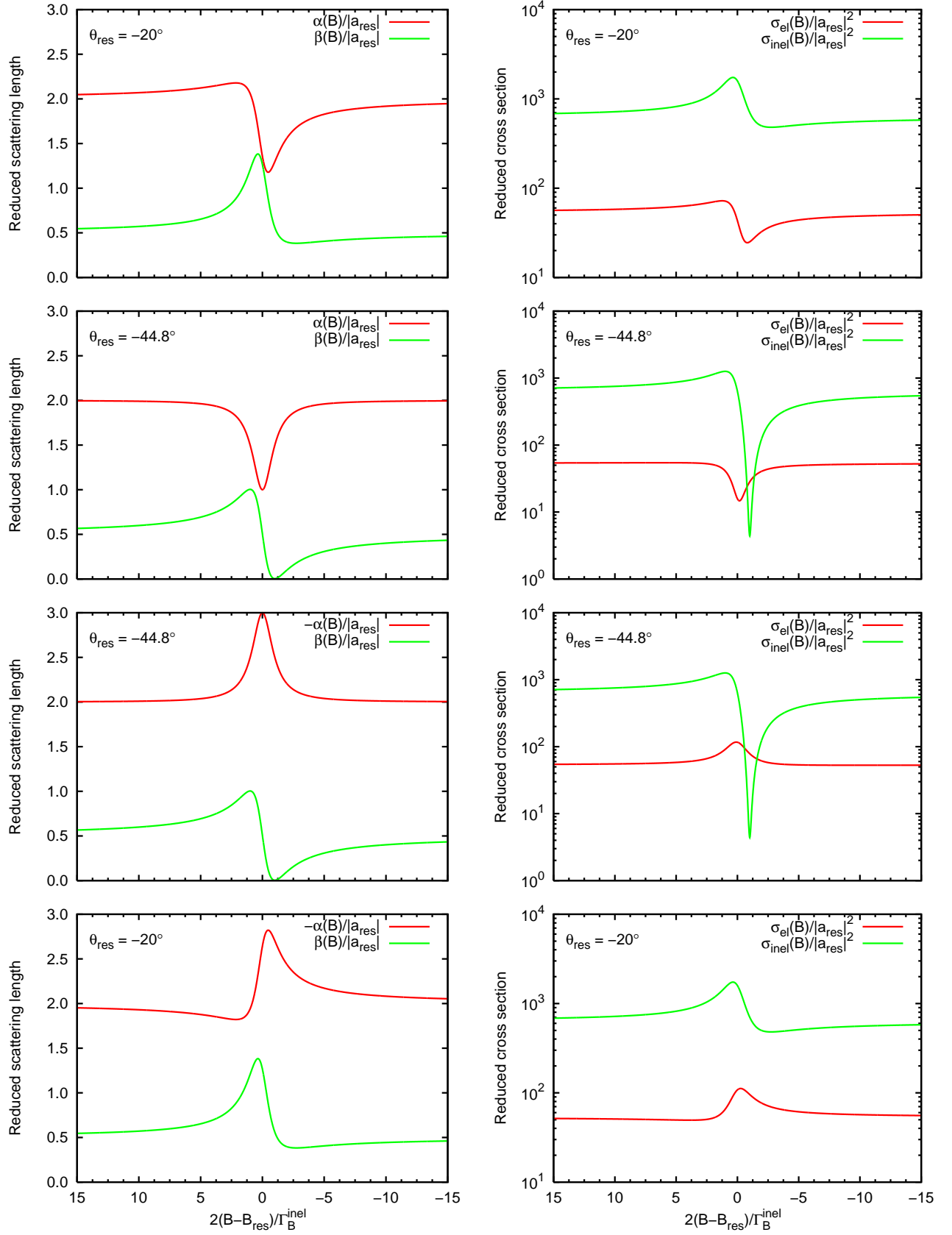


FIG. 5: (Color online). Some examples of the possible behavior for a case with moderately strong background inelasticity, $\beta_{bg} = |a_{res}|/2$ and $|\alpha_{bg}| = 2|a_{res}|$. The left-hand side shows the real and imaginary parts of the scattering length and the right-hand side shows the elastic and total inelastic cross sections (with inelastic cross sections calculated for a wave vector $k_0 = 10^{-2}|a_{res}|^{-1}$). The 4 panels show (from top to bottom): (i) positive α_{bg} , $\theta_{res} = -20^\circ$; (ii) positive α_{bg} , $\theta_{res} = 44^\circ$; (iii) negative α_{bg} , $\theta_{res} = -44^\circ$; (iv) negative α_{bg} , $\theta_{res} = -20^\circ$.

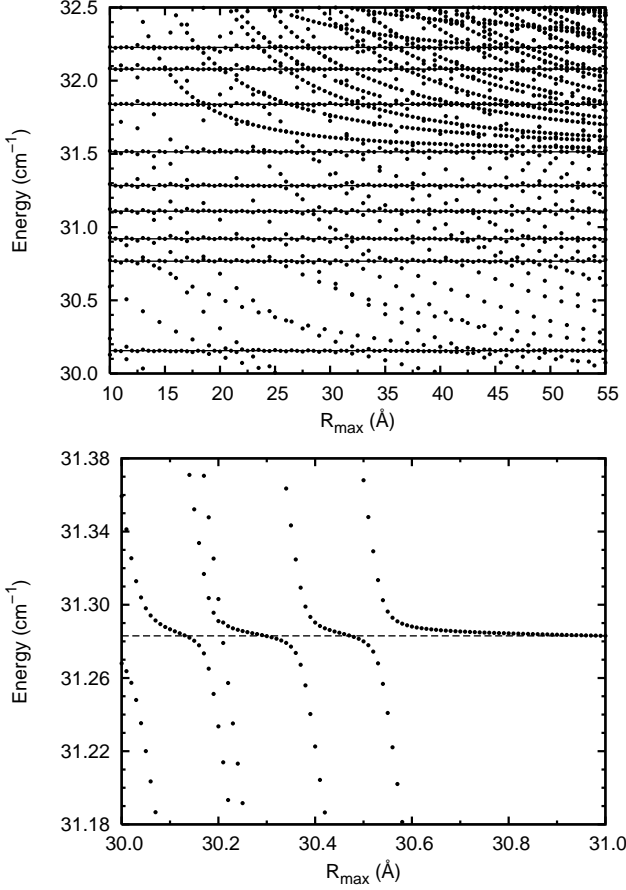


FIG. 6: The pattern of levels from bound-state calculations on He-NH near the $n = 1$ threshold as a function of R_{\max} . The calculations are for $B = 4000$ G, even parity, $M_{\text{tot}} = 0$. Note the artificial bound states with energies that decrease with R_{\max} , crossing and interfering with the physical states at constant energy. The lower panel shows a more detailed scan across a small region of R_{\max} showing avoided crossings between real and artificial states.

for He-NH each (n, j, L) level splits into $\min(2j+1, 2L+1)$ components with different values of J . These splittings are barely visible in Fig. 7, so Fig. 8 shows an expanded view of the levels corresponding to $(n, j, L) = (1, 1, 2)$ for all allowed values of M_{tot} . It may be seen that the zero-field levels with $J = 1, 2$ and 3 are split by about 0.04 cm^{-1} . When a magnetic field is applied, each level splits into $2J + 1$ components with different values of M_{tot} . The J quantum number remains a useful label for magnetic fields up to about 200 G, but above that the levels of different J are strongly mixed. By about 600 G the levels have separated into 3 groups that may be labelled with an approximate quantum number m_j that takes values $+1, 0$ and -1 . The levels corresponding to (n, j, L) show similar but more complex behavior.

Once the crossing points have been located in Fig. 7, the next stage is to carry out scattering calculations, holding the kinetic energy fixed at a small value (10^{-6} K in the present work) while sweeping the magnetic

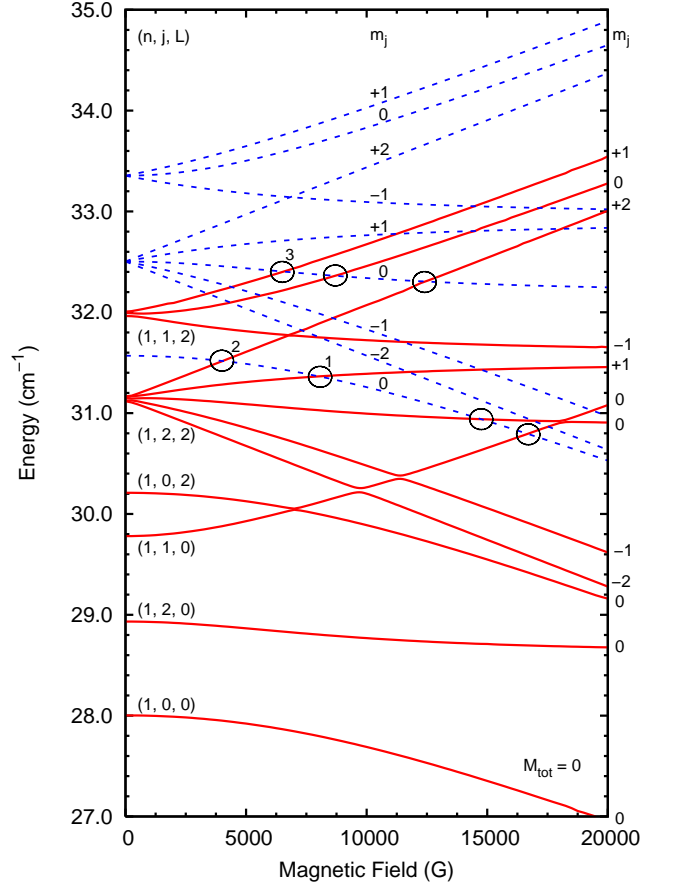


FIG. 7: (Color online). The pattern of levels from bound-state calculations on He-NH near the $n = 1$ threshold, with artificial levels removed, as a function of magnetic field B . The calculations are for even parity, $M_{\text{tot}} = 0$. The circles show crossings between bound states and thresholds that produce zero-energy Feshbach resonances.

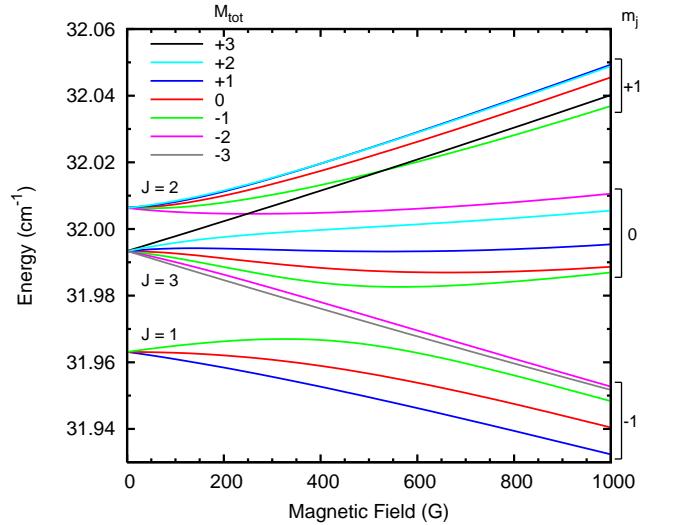


FIG. 8: (Color online). The pattern of He-NH levels arising from $(n, j, L) = (1, 1, 2)$ as a function of magnetic field B . The calculations are for even parity and all allowed values of M_{tot} .

field across the resonance. This was done using the MOLSCAT package [31], as modified to handle magnetic fields [29]. MOLSCAT solves the Schrödinger equation by propagating a set of coupled differential equations outwards from R_{\min} to a matching point R_{\max} at long range using basis sets and algorithms very similar to BOUND. The major difference is that it carries out only outwards propagation and matches to scattering boundary conditions at R_{\max} , so that there is no artificial quantization of the continuum.

MOLSCAT produces the S matrix and eigenphase sum Σ for each magnetic field B and evaluates the corresponding scattering length from Eq. 4. The next step is to fit $\Sigma(B)$ to Eq. 7 to obtain the resonance position B_{res} and width Γ_B . This is done with the RESFIT package [43], which includes a quadratic polynomial in B for the background term Σ_{bg} . RESFIT then proceeds to fit the individual diagonal S-matrix elements to Eq. 8, holding B_{res} and Γ_B fixed at the values obtained from the eigenphase sum. It represents the magnitude and phase of each S_{ii} with a quadratic polynomial and produces a complex number g_{Bi}^2 that describes the resonant circle in each S-matrix element. This fit provides all the parameters required to define the real and imaginary parts of a_{bg} and a_{res} needed for Eqs. 11 and 15. In practice we use a constant background term (obtained by evaluating the background polynomials at $B = B_{\text{res}}$) in plotting the results of the formulae below.

The results of fitting parameters to several resonances are shown in Table I. The first point to notice is that the resonances are all very wide, with $|\Gamma_B| > 30$ G. This contrasts with the $n = 0$ resonances previously characterized [29], which had $|\Gamma_B| < 10^{-2}$ G. The difference arises because the $n = 1$ closed channels involved here are directly coupled to $n = 0$ channels by the (weak) potential anisotropy, whereas the $n = 0$ closed channels involved in our previous work were only indirectly coupled to open channels by a second-order mechanism involving both the potential anisotropy and spin-spin coupling. The second point of interest is that a_{res} has a significant imaginary part in each case, with $\beta_{\text{res}}/\alpha_{\text{res}}$ considerably greater than $\beta_{\text{bg}}/\alpha_{\text{bg}}$. Because of this, there is significant asymmetry in the calculated resonant line shapes for $\alpha(B)$ and $\beta(B)$.

The real and imaginary scattering lengths for the resonance labelled 1 in Fig. 7 are shown in the upper panels of Fig. 9. In each case the black points show the numerical results from MOLSCAT and the red line shows the result of Eq. 11 with the assumption that a_{res} is real (i.e., a_{res} replaced by $|a_{\text{res}}|$). It may be seen that there are significant discrepancies, shown by the red lines in the two lower panels. By contrast, if a_{res} is allowed to be complex (Eq. 15), we obtain almost perfect fits to the numerical results except for the neglect of the field-dependence of the background scattering length a_{bg} . The result is too close to the points to show usefully in the upper panels of Fig. 9, but the difference between the MOLSCAT results and those given by Eq. 15 are shown as the blue lines in

Figs. 9.

These results verify that Eq. 15 gives a correct account of the behavior of the scattering length in the presence of significant (but still small) background inelastic scattering. The complex nature of a_{res} manifests itself in a slight tilting of the circles in the S-matrix elements, as shown in Fig. 3. The tilt is too small to be shown graphically, but may be seen in the numerical values in Table I.

The asymmetries seen in Fig. 9 are much smaller than the possible asymmetries shown in Fig. 5, but they nevertheless serve to illustrate the principle that resonant signatures can be asymmetric and that inelastic cross sections can show troughs as well as peaks near resonance. In future work we will investigate systems with stronger background inelasticity in which more dramatic asymmetries can be expected.

A. Computational details

The bound and scattering calculations in the present work used a basis set with $n_{\max} = 5$ and $L_{\max} = 5$. The coupled equations were solved using Johnson's log-derivative algorithm [44] with $R_{\min} = 1.7$ Å and a step size of 0.025 Å. The bound-state calculations used $R_{\max} = 12$ Å except where stated otherwise, and the scattering calculations used $R_{\max} = 100$ Å.

III. CONCLUSIONS

We have investigated the behavior of low-energy Feshbach resonances for a case where there is significant background inelastic scattering far from resonance. We have located low-energy Feshbach resonances in s-wave scattering of NH ($^3\Sigma^-$, $n = 1$) with He. The resonances are much wider ($\Gamma_B > 30$ G) than those found previously for scattering of NH ($n = 0$) ($\Gamma_B < 10^{-2}$ G) [29]. We have investigated how scattering lengths and cross sections vary as a resonance is tuned across threshold using an external magnetic field.

The strength of a resonance can be characterized by a *resonant scattering length* a_{res} . If only elastic scattering is possible, a_{res} is infinite and the scattering length passes through a pole as a bound state crosses threshold. We have shown previously [29] that this behavior is modified in the presence of inelastic collisions and that in some cases the scattering length shows a small oscillation rather than a pole.

The key result of the present paper is the demonstration that a_{res} can be complex rather than real and that this allows both the real and imaginary parts of the scattering length (and thus elastic and inelastic cross sections) to show both peaks and troughs near resonance. We have shown that the real and imaginary parts of the scattering length follow analytical formulas given previously [32].

Resonance	M_{tot}	B_{res} (G)	Γ_B^{inel} (G)	Γ_{B0} (10^{-2} G)	α_{bg} (Å)	β_{bg} (10^{-3} Å)	α_{res} (Å)	β_{res} (10^{-2} Å)	θ_{res}
1	0	8154.71	-56.19	-3.938	3.2016	4.21	2.1735	9.08	-0.0278
2	0	4078.47	-52.21	-3.208	3.2355	5.72	1.9057	8.57	-0.0225
3	0	6644.15	-56.95	-2.224	3.1929	4.72	1.2119	4.76	-0.0196
4	-2	4250.00	-33.64	-2.804	3.1931	4.50	2.5856	10.04	-0.0194

TABLE I: Parameters of magnetically tuned Feshbach resonances in He + NH ($n = 1$) collisions at $E_{\text{kin}} = 10^{-6}$ K, corresponding to $k_0 = 3.2189 \times 10^{-4} \text{ Å}^{-1}$. Resonances 1 to 3 correspond to the correspondingly numbered circles in Fig. 7, while resonance 4 is for a different value of M_{tot} .

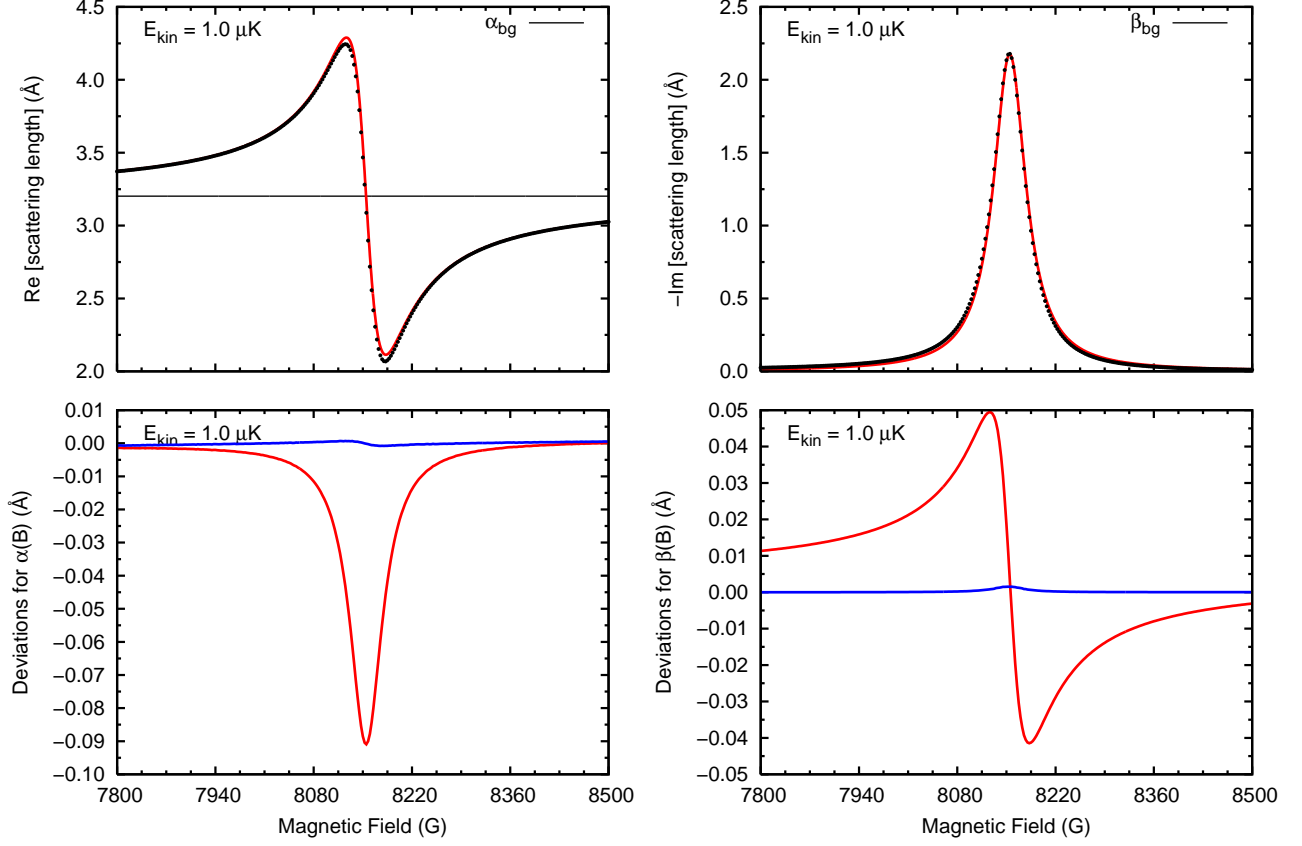


FIG. 9: (Color online). Upper panels: the real (left) and imaginary (right) parts of the scattering length for resonance 1 as a function of magnetic field. The black dots show numerical results from MOLSCAT and the red line shows the result of using Eq. (11) with a real value of a_{res} . Lower panel: deviations between the numerical results and the formula using real (red, Eq. 11) and complex (blue, Eq. 15) values of a_{res} .

The present work offers the hope that tuning close to a Feshbach resonance can be used to reduce inelastic collision rates and thereby allow evaporative or sympathetic cooling in cases where collisional trap losses would otherwise prevent it. In future work we will investigate whether additional influences such as electric fields can be used to *control* the maxima and minima and allow detailed control of collision rates.

Acknowledgments

The authors are grateful to the EPSRC for funding under grant EP/E039200/1 and to the Royal Society for an International Joint Project grant which made this collaboration possible.

[1] J. M. Hutson and P. Soldán, Int. Rev. Phys. Chem. **25**, 497 (2006).

[2] T. Köhler, K. Goral, and P. S. Julienne, Rev. Mod. Phys. **78**, 1311 (2006).

- [3] J. L. Roberts, N. R. Claussen, S. L. Cornish, E. A. Donley, E. A. Cornell, and C. E. Wieman, *Phys. Rev. Lett.* **86**, 4211 (2001).
- [4] E. A. Donley, N. R. Claussen, S. T. Thompson, and C. E. Wieman, *Nature* **417**, 529 (2002).
- [5] J. Herbig, T. Kraemer, M. Mark, T. Weber, C. Chin, H. C. Nägerl, and R. Grimm, *Science* **301**, 1510 (2003).
- [6] K. Xu, T. Mukaiyama, J. R. Abo-Shaeer, J. K. Chin, D. E. Miller, and W. Ketterle, *Phys. Rev. Lett.* **91**, 210402 (2003).
- [7] S. Dürr, T. Volz, A. Marte, and G. Rempe, *Phys. Rev. Lett.* **92**, 020406 (2004).
- [8] C. A. Regal, C. Ticknor, J. L. Bohn, and D. S. Jin, *Nature* **424**, 47 (2003).
- [9] K. E. Strecker, G. B. Partridge, and R. G. Hulet, *Phys. Rev. Lett.* **91**, 080406 (2003).
- [10] J. Cubizolles, T. Bourdel, S. J. J. M. F. Kokkelmans, G. V. Shlyapnikov, and C. Salomon, *Phys. Rev. Lett.* **91**, 240401 (2003).
- [11] S. Jochim, M. Bartenstein, A. Altmeyer, G. Hendl, C. Chin, J. H. Denschlag, and R. Grimm, *Phys. Rev. Lett.* **91**, 240402 (2003).
- [12] S. Jochim, M. Bartenstein, A. Altmeyer, G. Hendl, S. Riedl, C. Chin, J. H. Denschlag, and R. Grimm, *Science* **302**, 2101 (2003).
- [13] M. W. Zwierlein, C. A. Stan, C. H. Schunck, S. M. F. Raupach, S. Gupta, Z. Hadzibabic, and W. Ketterle, *Phys. Rev. Lett.* **91**, 250401 (2003).
- [14] M. Greiner, C. A. Regal, and D. S. Jin, *Nature* **426**, 537 (2003).
- [15] T. Kraemer, M. Mark, P. Waldburger, J. G. Danzl, C. Chin, B. Engeser, A. D. Lange, K. Pilch, A. Jaakkola, H. C. Nägerl, et al., *Nature* **440**, 315 (2006).
- [16] C. Chin, T. Kraemer, M. Mark, J. Herbig, P. Waldburger, H. C. Nägerl, and R. Grimm, *Phys. Rev. Lett.* **94**, 123201 (2005).
- [17] M. Mark, T. Kraemer, P. Waldburger, J. Herbig, C. Chin, H.-C. Naegerl, and R. Grimm, *arXiv:cond-mat/0704.0653* (2007).
- [18] M. Mark, F. Ferlaino, S. Knoop, T. Kraemer, C. Chin, H.-C. Naegerl, and R. Grimm, *arXiv:cond-mat/0706.1041* (2007).
- [19] C. J. Pethick and H. Smith, *Bose-Einstein Condensation in Dilute Gases* (Cambridge University Press, 2002).
- [20] A. J. Moerdijk, B. J. Verhaar, and A. Axelsson, *Phys. Rev. A* **51**, 4852 (1995).
- [21] J. D. Weinstein, R. deCarvalho, T. Guillet, B. Friedrich, and J. M. Doyle, *Nature* **395**, 148 (1998).
- [22] D. Egorov, W. C. Campbell, B. Friedrich, S. E. Maxwell, E. Tsikata, L. D. van Buuren, and J. M. Doyle, *Eur. Phys. J. D* **31**, 307 (2004).
- [23] W. C. Campbell, E. Tsikata, L. van Buuren, H.-I. Lu, and J. M. Doyle, *arXiv:physics/0702071* (2007).
- [24] H. L. Bethlem and G. Meijer, *Int. Rev. Phys. Chem.* **22**, 73 (2003).
- [25] H. L. Bethlem, M. R. Tarbutt, J. Küpper, D. Carty, K. Wohlfart, E. A. Hinds, and G. Meijer, *J. Phys. B – At. Mol. Opt. Phys.* **39**, R263 (2006).
- [26] P. Domokos and H. Ritsch, *Phys. Rev. Lett.* **89**, 253003 (2002).
- [27] H. W. Chan, A. T. Black, and V. Vuletic, *Phys. Rev. Lett.* **90**, 063003 (2003).
- [28] G. Morigi, P. W. H. Pinkse, M. Kowalewski, and R. de Vivie-Riedle, *arXiv:quant-ph/0703157* (2007).
- [29] M. L. González-Martínez and J. M. Hutson, *Phys. Rev. A* **75**, 022702 (2007).
- [30] J. M. Hutson, *Bound computer program, version 5*, distributed by Collaborative Computational Project No. 6 of the UK Engineering and Physical Sciences Research Council (1993).
- [31] J. M. Hutson and S. Green, *Molscat computer program, version 14*, distributed by Collaborative Computational Project No. 6 of the UK Engineering and Physical Sciences Research Council (1994).
- [32] J. M. Hutson, *New J. Phys.* **9**, 152 (2007), note that there is a typographical error in Eq. (22) of this paper: the last term on the right-hand side should read $-\beta_{\text{res}}$ instead of $+\beta_{\text{res}}$.
- [33] N. F. Mott and H. S. W. Massey, *The Theory of Atomic Collisions* (Clarendon Press, Oxford, 1965), 3rd ed.
- [34] J. L. Bohn and P. S. Julienne, *Phys. Rev. A* **56**, 1486 (1997).
- [35] N. Balakrishnan, V. Kharchenko, R. C. Forrey, and A. Dalgarno, *Chem. Phys. Lett.* **280**, 5 (1997).
- [36] M. T. Cvitaš, P. Soldán, J. M. Hutson, P. Honvault, and J. M. Launay, *arXiv:physics/0703136* (2007).
- [37] A. U. Hazi, *Phys. Rev. A* **19**, 920 (1979).
- [38] C. J. Ashton, M. S. Child, and J. M. Hutson, *J. Chem. Phys.* **78**, 4025 (1983).
- [39] W. Brenig and R. Haag, *Fortschr. Phys.* **7**, 183 (1959).
- [40] J. R. Taylor, *Scattering Theory: The Quantum Theory of Nonrelativistic Collisions* (Wiley, New York, 1972).
- [41] B. Gazdy and J. M. Bowman, *Phys. Rev. Lett.* **59**, 3 (1987).
- [42] J. M. Hutson, *Comput. Phys. Commun.* **84**, 1 (1994).
- [43] J. M. Hutson, *Resfit 2007 computer program* (2007).
- [44] B. R. Johnson, *J. Comput. Phys.* **13**, 445 (1973).